Icarus 215 (2011) 346–357

Contents lists available at ScienceDirect

Icarus

journal homepage: www.elsevier.com/locate/icarus

Origin of the martian dichotomy and Tharsis from a giant impact causing massive magmatism

Gregor J. Golabek [a,b,*], Tobias Keller [a], Taras V. Gerya [a], Guizhi Zhu [a], Paul J. Tackley [a], James A.D. Connolly [c]

[a] Institute of Geophysics, ETH Zürich, 8092 Zürich, Switzerland
[b] Laboratoire des Sciences de la Terre, ENS Lyon, 69364 Lyon Cedex 07, France
[c] Institute of Geochemistry and Petrology, ETH Zürich, 8092 Zürich, Switzerland

ARTICLE INFO

Article history:
Received 11 February 2011
Revised 3 June 2011
Accepted 9 June 2011
Available online 22 June 2011

Keywords:
Geophysics
Mars
Planetary formation
Planetary dynamics

ABSTRACT

The origin of the ancient martian crustal dichotomy and the massive magmatic province of Tharsis remains an open problem. Here, we explore numerically a hypothesis for the origin of these two features involving both exogenic and endogenic processes. We propose a giant impact event during the late stage of planetary formation as the source of the southern highland crust. In a second stage, the extraction of excess heat by vigorous mantle convection on the impacted hemisphere leads to massive magmatism, forming a distinct Tharsis-like volcanic region. By coupling short-term and long-term numerical simulations, we are able to investigate both the early formation as well as the 4.5 Gyr evolution of the martian crust. We demonstrate numerically that this exogenic–endogenic hypothesis is in agreement with observational data from Mars.

1. Introduction

Along with the crustal dichotomy (McCauley et al., 1972), the martian surface is dominated by the massive volcanic region of Tharsis, featuring the largest shield volcanoes in the Solar System. Although the youngest volcanism on Tharsis can be dated to recent geological times (Neukum et al., 2004; Werner, 2009; Carr and Head, 2010; Niles et al., 2010), the bulk of Tharsis was emplaced at the latest 3.7 Ga ago (Phillips et al., 2001; Solomon et al., 2005; Werner, 2009; Carr and Head, 2010; Hauber et al., 2010). Thus, it was suggested that the formation of Tharsis likely is directly linked to the crustal dichotomy and its origin (Nimmo and Tanaka, 2005). Here we explore a two-stage hypothesis suggesting an impact-induced shallow magma ocean as the primary source of the southern highland crust. Subsequently, the left-over thermal anomaly in the martian mantle triggers a transient superplume on the impacted hemisphere, leading to the formation of a large volcanic province, such as Tharsis.

The bulk of the martian crust and its features are ancient. Based on geochemical measurements, it has been proposed that at least one third, but probably even the majority of the martian crust, was already formed during martian core formation (Norman, 1999; Taylor and McLennan, 2009). Following geological evidence, the martian dichotomy was emplaced at the latest 400–500 Ma after planetary formation (Nimmo and Tanaka, 2005; Solomon et al., 2005; Frey, 2006; Werner, 2009; Carr and Head, 2010). The exogenic approach to the origin of the crustal dichotomy (Wilhelms and Squyres, 1984; Frey and Schultz, 1988; Andrews-Hanna et al., 2008; Marinova et al., 2008; Nimmo et al., 2008) assumes that the northern lowlands correspond to a giant impact basin formed after primordial crust formation. The presence of buried impact craters on the northern hemisphere (Frey, 2006), indicating a similar crustal age for both hemispheres, however, poses a serious problem to this view. The endogenic approach (e.g., Weinstein, 1995), suggesting a degree-1 mantle upwelling underneath the southern highlands (Zhong and Zuber, 2001; Roberts and Zhong, 2006; Zhong, 2009; Keller and Tackley, 2009; Šrámek and Zhong, 2010), relies on a high Rayleigh number and a particular viscosity profile to form a low degree convective planform within the geological constraints for the dichotomy formation. Such vigorous convection, however, results in continuous magmatic resurfacing, destroying the initially dichotomous crustal structure in the long-term.

The hybrid exogenic–endogenic approach (Reese and Solomatov, 2006, 2010; Reese et al., 2010), proposing an impact-induced magma ocean and subsequent superplume in the southern hemisphere, is in closer agreement (Reese et al., 2010) with the inferred crustal ages (Frey, 2006). It has, however, only been discussed in terms of a simplified thermo-mechanical model, without actual simulation of the crustal formation and long-term evolution resulting from the magma ocean and the superplume. In this hypothesis, the formation of the crustal dichotomy takes

* Corresponding author at: Laboratoire des Sciences de la Terre, ENS Lyon, 69364 Lyon Cedex 07, France.
E-mail address: gregor.golabek@ens-lyon.fr (G.J. Golabek).

0019-1035/$ - see front matter © 2011 Elsevier Inc. All rights reserved.
doi:10.1016/j.icarus.2011.06.012

place either simultaneously or immediately subsequent to accretion and core formation.

Current understanding indicates that accretion of larger terrestrial bodies by stochastically distributed impacts and their differentiation into mantle and core occur simultaneously (e.g., Raymond et al., 2006; Rubie et al., 2007). From numerical N-body simulations, accretion of Mars and therefore also its iron core formation, are thought to have been completed after about 10 Ma (Raymond et al., 2006). Geochemical data of the hafnium–tungsten isotopic system also support a martian accretion time scale of 0–10 Ma (Nimmo and Kleine, 2007).

Towards the end of terrestrial planetary accretion, giant impacts are inevitable. It has been estimated that the largest impactors during martian accretion history should have had masses of about 0.1–1 times the lunar mass, corresponding to impactor radii of around 800–1700 km (Reese and Solomatov, 2006, 2010; Reese et al., 2010). However, if Mars itself is a leftover planetary embryo (Wetherill, 1992; Chambers and Wetherill, 1998) then the impacts large enough to cause significant silicate melting would be very few and would most likely take place late in martian accretion history. Our hypothesis suggests that the last of these giant impacts, occurring during the late stage of accretion and ongoing core formation, would induce a strong asymmetry in the planet's thermal structure responsible for the crustal features under discussion.

Such an event would cause large amounts of silicate melting at the surface, most likely to the extent that a hemispherical magma ocean forms (Reese and Solomatov, 2006, 2010; Reese et al., 2010). Subsequently, both the onset of mantle convection (Reese et al., 2002) as well as the spatial distribution of primordial crust would be significantly influenced by this event. Moreover, it is likely that the crust generated from the hemispherical magma ocean formed by the last giant impact would be largely preserved and only disrupted locally by few, notably smaller impactors forming basins like Hellas during the later planetary evolution. Neither will the thermal anomaly be leveled out by intense radiogenic heating, as short-lived radiogenic isotopes will largely have decayed by the time of this giant impact. Therefore, the signature of such an event would likely be preserved both on the surface and in the interior of the planet.

The structure of this paper is as follows: Section 2 gives an overview of the methodology applied in this study and Section 3 describes the model setup. Sections 4 and 5 present the results and the discussion, respectively.

2. Methods

We consider two-dimensional creeping flow using the extended Boussinesq approximation, including both thermal and chemical buoyancy forces. To fully capture the diversity of processes, we serially couple the two finite-difference codes I2ELVIS (Gerya and Yuen, 2007) for core formation and STAGYY (Tackley, 2008; Hernlund and Tackley, 2008) for the onset of mantle convection and crust formation. The thermal end state of the former simulation gives the initial condition for the latter. We assume a temperature-, pressure-, strain-rate and melt fraction-dependent viscoplastic rheology for silicate material. Features not given in the publications mentioned above documenting the corresponding code, will be described below.

2.1. I2ELVIS

2.1.1. Impact treatment

A simplified model is used to take into account the thermal anomaly and the presence of a giant impactor iron core in the mantle of the target body. Effects like accretion of silicate material from the impactor, the redistribution of target material around the planetary body by crater excavation and possible decompression melting after transient crater collapse are not taken into account.

For the giant impact, the radius of the isobaric core (Croft, 1982) – a region of approximately the same shock pressure and therefore almost uniform post-impact temperature increase – is based on a parametrization (Senshu et al., 2002):

$$R_{ic} = 3^{1/3} r_{imp} \tag{1}$$

where R_{ic} is the radius of the isobaric core and r_{imp} is the total impactor radius.

The thermal anomaly in the isobaric core ΔT is calculated as follows (Monteux et al., 2007):

$$\Delta T = \frac{4\pi}{9}\frac{\psi}{F}\frac{\rho_p G R_P^2}{c_p} \tag{2}$$

$\psi$is the efficiency of conversion of kinetic energy to thermal energy assumed to be 0.3 (O'Keefe and Ahrens, 1977). F is a function representing the volume effectively heated normalized by the volume of the isobaric core. Its value was suggested to be close to 2.7 (Monteux et al., 2007). ρ_P is the mean density of the target planetary body with radius R_P. Finally G and c_p are the gravitational constant and the heat capacity of the target body, respectively.

The thermal anomaly is superimposed on the previous temperature structure of the planetary body. The model assumes that the center of the isobaric core is identical to the center of the impactor iron core. Outside of the isobaric core ($r > R_{ic}$) the thermal anomaly due to the impact decays exponentially and can be described as follows (Senshu et al., 2002; Monteux et al., 2007):

$$T(r) = \Delta T\left(\frac{R_{ic}}{r}\right)^{4.4} \tag{3}$$

2.1.2. Batch melting model for silicates

A batch-melting model assuming a dry peridotite composition is included. The martian mantle contains more iron than Earth's, however its influence on the location of the solidus is negligible (Hirschmann, 2000). Thus, parametrizations for both the solidus and liquidus temperature T_{sol} and T_{liq} of peridotite assuming an Earth-like composition can be applied (Hirschmann, 2000; Wade and Wood, 2005).

For $T \leqslant T_{sol}$ the melt fraction ϕ is zero, for $T \geqslant T_{liq}$ it is equal 1. In the intermediate temperature range $T_{sol} < T < T_{liq}$, the melt fraction is assumed to increase linearly with temperature accordingly to the following relation (Burg and Gerya, 2005):

$$\phi = \frac{(T - T_{sol})}{(T_{liq} - T_{sol})} \tag{4}$$

Consequently, the effective density ρ_{eff} of partially molten rocks varies with the amount of melt ϕ, additionally to its dependence on the temperature (T) and pressure (P) conditions and composition c (see Gerya and Yuen, 2007). The effective density is assumed to vary linearly with the melt fraction (Burg and Gerya, 2005):

$$\rho_{eff}(c,P,T,\phi) = \rho_{Si\text{-}sol}(c,P,T) - \phi[\rho_{Si\text{-}sol}(c,P,T) - \rho_{Si\text{-}liq}(c,P,T)] \tag{5}$$

where $\rho_{Si\text{-}sol}$ and $\rho_{Si\text{-}liq}$ are the densities of the solid and liquid silicates, respectively.

The presence of a melt fraction $\phi > 0.1$ also has an influence on the effective viscosity of the silicate material η_{eff}, which is described as follows (Pinkerton and Stevenson, 1992):

$$\eta_{eff}(\phi) = \eta_{Si\text{-}liq}\ exp\left\{\left[2.5 + \left(\frac{1-\phi}{\phi}\right)^{0.48}\right](1-\phi)\right\} \tag{6}$$

where $\eta_{Si\text{-}liq}$ is the viscosity of the molten silicate material.

2.1.3. Estimation of the effective thermal conductivity of the magma ocean

The viscosity of largely molten silicates is expected to be $\eta_{Si\text{-}liq} \approx 0.1$–100 Pa s (Bottinga and Weill, 1972; Liebske et al., 2005). Hence, due to the low viscosity, both the Rayleigh and the Nusselt number will be very high and cooling will be very efficient. Even deep magma oceans are therefore expected to freeze out in 0.1–1 Ma (Solomatov, 2007). However due to numerical restrictions, the lower cut-off viscosity in the model is $\eta_{num} = 10^{17}$ Pa s, orders of magnitude higher than realistic melt viscosities. Taking the dependency of the effective viscosity of partially molten silicates on temperature T, strain-rate $\dot{\epsilon}$ and melt-fraction ϕ (see Gerya and Yuen, 2007) into account, we can expect that the effective viscosity is close to the cut-off viscosity value. It was suggested that the heat flux from a magma ocean (Solomatov, 2007) can be described using the so-called soft turbulence model (Kraichnan, 1962; Siggia, 1994). In this model the expected convective heat flux q is given as:

$$q = 0.089 \frac{k(T - T_{surf})}{L} Ra^{1/3} \tag{7}$$

where Ra is the Rayleigh number given by:

$$Ra = \frac{\alpha g (T - T_{surf}) \rho_{Si\text{-}liq}^2 c_P L^3}{k \eta_{Si\text{-}liq}} \tag{8}$$

α is the thermal expansivity, g is the gravitational acceleration, T is the potential temperature, T_{surf} is the surface temperature, k is the thermal conductivity and L is the depth of the magma ocean.

Depending on the actual silicate melt viscosity of the numerical model η_{num}, we can estimate an increased effective thermal conductivity k_{eff} by using the expected heat flux q from above. This effective thermal conductivity can simulate the heat flux of a medium with real magma ocean viscosity (Tackley et al., 2001). This can be done using the following expression for the effective thermal conductivity k_{eff}:

$$k_{eff} = \left(\frac{q}{0.089}\right)^{3/2} \frac{1}{(T - T_{surf})^2 \rho_{Si\text{-}liq}} \left(\frac{\alpha g c_P}{\eta_{num}}\right)^{-1/2} \tag{9}$$

Using parameters from Table 1, expected values range between $k_{eff} \sim 9.5 \times 10^7$ and 3×10^9 W m^{-1} K^{-1}.

Furthermore, we have to take into account that spreading of the molten layer in our model is limited by its higher viscosity compared to a real magma ocean. Following estimations (Griffiths and Fink, 1993; Reese and Solomatov, 2006), the spreading distance of a magma ocean from its source over the planetary surface S is given by:

$$S \sim \pi^{-3/8} \left(\frac{\rho_{Si\text{-}liq} g V^3}{\eta_{Si\text{-}liq}}\right)^{1/8} t^{1/8} \tag{10}$$

where V is the volume of partial and complete melt available and t is the time.

In the numerical model all parameters except the silicate melt viscosity, are the same as in a real magma ocean. Hence, for the same time of spreading, the ratio between spreading distance for real molten silicates S_{real} and the numerical molten silicates S_{num} is, dependent on the viscosity of the molten silicates (see above), given as:

$$\frac{S_{real}}{S_{num}} \sim \left(\frac{\eta_{num}}{\eta_{Si\text{-}liq}}\right)^{1/8} \sim 75\text{–}237 \tag{11}$$

Thus, to allow the magma ocean in the numerical model to traverse a similar distance as in nature, the timescale until magma ocean freezing has to be increased in the model compared to nature by reducing the effective thermal conductivity. This timescale is inversely proportional to the heat flux q (Reese and Solomatov, 2006). The heat flux (see combined Eqs. (7) and (8)) is dependent on the thermal conductivity as $q \sim k^{2/3}$. We derive values k_{eff} of 1.5–8 $\times 10^5$ W m^{-1} K^{-1} for molten silicates taking both a rapid freezing and the distance effect into account.

2.1.4. Phase changes

Densities of silicate material are self-consistently calculated with the Perple_X package (Connolly, 2005), using the minimization of Gibbs free energy for the corresponding P–T conditions to determine stable minerals for a Mars-like mantle composition (Khan and Connolly, 2008). Latent heat associated with phase changes is considered in the numerical model.

Table 1
Model parameters.

Parameter	Symbol	Value	Units
Radius of planetary body	R_P	3.4×10^6	m
Density of uncompressed solid silicates	$\rho_{Si\text{-}sol}$	3500	kg m^{-3}
Density of uncompressed silicate melt	$\rho_{Si\text{-}liq}$	2900	kg m^{-3}
Density of uncompressed iron	ρ_{Fe}	8000	kg m^{-3}
Mantle basalt fraction after core formation	f_{bas}	0.15	
Cohesion	χ	10^8	Pa
Friction angle	$sin(i)$	0.6	
Peierls stress	σ_P	9.1×10^9	Pa
Activation energy	E_a	532	kJ mol^{-1}
Activation volume	V_a	8.0×10^{-6}	m^3 mol^{-1}
Dislocation creep onset stress	σ_0	3.0×10^7	Pa
Power law exponent	n	3.5	
Latent heat of melting	L	400	kJ kg^{-1}
Heat capacity of silicate materials	c_P	1000	J kg^{-1} K^{-1}
Heat capacity of iron material	c_{P-Fe}	800	J kg^{-1} K^{-1}
Thermal expansivity of solid silicates	$\alpha_{Si\text{-}sol}$	3.0×10^{-5}	K^{-1}
Thermal expansivity of molten silicates	$\alpha_{Si\text{-}liq}$	6.0×10^{-5}	K^{-1}
Thermal expansivity of iron material	α_{Fe}	1.0×10^{-5}	K^{-1}
Thermal conductivity of solid materials	k	3.0	W m^{-1} K^{-1}
Thermal conductivity of iron material	k_{Fe}	38.4	W m^{-1} K^{-1}
Effective thermal conductivity of molten materials	k_{eff}	3.0×10^5	W m^{-1} K^{-1}
Crustal radiogenic heating enrichment factor	Λ	10	

2.2. Computation of a primordial crust

A primordial crust resulting from the freezing of the surface magma ocean is computed in a post-processing step from I2ELVIS results. Thus, the melt extraction has no influence on the dynamics of core formation. For this purpose the silicate melt distribution is tracked on the markers of the corresponding I2ELVIS model. The Cartesian coordinates of the markers are transformed into polar coordinates (Bronstein et al., 2001). The number of crust bins in which crustal thickness is sampled is given by the radial resolution of the mantle convection simulation to follow.

The following criteria are assumed for partially molten markers to contribute to crustal production:

(a) Marker is freezing between timesteps t_1 and $t_2 > t_1$ and its melt fraction $\Delta\phi$ drops below 20%. Only the difference in melt fraction below 20%, in an already largely frozen magma ocean, is counted as material contributing to crust formation. This corresponds roughly to the pyroxene fraction of a fertile mantle, which again is the main component in the basaltic to andesitic composition of the crust that is being formed (McKenzie and Bickle, 1988).
(b) The melt on a marker is positively buoyant and thus would rise to the surface to form crust (a neutral buoyancy depth of ~600 km is assumed (Breuer and Spohn, 2006; Suzuki et al., 1998)).

Each marker represents an area A_{crust} of

$$A_{crust} = \frac{d_x d_z}{[(N_x - 1)m_x(N_z - 1)m_z]} \tag{12}$$

where d_x and d_z are the dimensions of the numerical box in x and z direction, whereas N_x and N_z are the numbers of grid points in x and z direction in the I2ELVIS model. Finally m_x and m_z are the number of markers per grid cell used by I2ELVIS in both x and z direction.

The area fraction of freezing melt is projected onto the surface of the planet and fills corresponding bins. In case a marker does not change its position between time t_1 and t_2, yet fulfils the criteria discussed above, a minimum angle $\Delta\alpha$ of one degree is used for crust formation. Crustal production is an ineffective process due to partial crystallization of percolating melts. Thus it is assumed that only 50% of the freezing melt can contribute to crust formation. The thickness of the newly produced crust d_{crust} is calculated as:

$$d_{crust} = R_P - \sqrt{R_P^2 - \left(\frac{360}{\Delta\alpha}\frac{a_{eff}\Delta\phi A_{crust}}{\pi}\right)} \tag{13}$$

where $\Delta\alpha = \max(1^\circ, |\alpha_{old} - \alpha_{new}|)$, where α_{old} and α_{new} are the angular coordinate of the previous and the current time step, respectively. R_P is the radius of the planetary body, a_{eff} is the efficiency of crustal production and $\Delta\phi$ is the melt fraction available for crust formation.

This procedure is repeated for all markers fulfilling the above criteria and the crustal production in each bin is stacked over time. The crust is assumed to be erupted instantly to the surface and to be unaffected by crustal recycling back into the magma ocean, reasonable for the low melt fractions and effective silicate viscosities of about 10^{17} Pa s (Reese et al., 2010) expected toward the end of magma ocean freezing. As the depth of the spreading magma ocean is larger in the center of the originally impacted region a thicker primordial crust can form there. The usage of different numbers of bins does not affect the crustal distribution significantly. Therefore this method is robust in providing a first order approximation of the upper limit of primordial crustal production. The resulting crustal distribution is finally read into the mantle convection simulation as an input file.

2.3. STAGYY

2.3.1. Phase transitions

In the STAGYY model both the olivine and the garnet-pyroxene fraction of the martian mantle material are taken into account based on martian compositional data (Bertka and Fei, 1997). The olivine mineralogical system has a volume fraction of $v_{ol} = 0.55$, the garnet/pyroxene system has a fraction of $v_{gt/px} = 0.45$. Phase transitions in both mineralogical systems are considered. The presence of a certain phase at the point of interest is defined by the Clapeyron slope of that certain phase transition and the depth d (assuming hydrostatic pressure) and temperature T at that point. The position, deflection and sharpness for each of these transitions is computed using the phase function Γ:

$$\Gamma_{ij} = \frac{1}{2}\left[1 + \tanh\left[\frac{(d - d_{ij}) - \gamma_{ij}(T - T_{ij})}{w_{ij}}\right]\right] \tag{14}$$

d_{ij} and T_{ij} are the reference depth and temperature of the i-th phase transition of the mineralogical system j, respectively. γ_{ij} is the Clapeyron slope and w the width over which a phase transition takes place (see also Table 2). The widths of the phase transitions are chosen as to reflect the nature of the respective mineralogical processes (Keller and Tackley, 2009).

It was suggested that a viscosity increase with depth effectively reduces the degree of martian mantle convection (Roberts and Zhong, 2006; Keller and Tackley, 2009). Experiments indicate that high-pressure silicate minerals show higher viscosities than their low pressure counterparts (Meade and Jeanloz, 1990). Thus, we implement a total viscosity increase $\Delta\eta$ of factor 60 over all phase transformations (see also Table 2). This dependency of viscosity η on composition c is implemented as:

$$\eta(c, P, T) = \eta(P, T)\sum_{ij}[\Delta\eta_{ij}]^{\Gamma_{ij} v_j} \tag{15}$$

$j = 1$ stands for the olivine mineralogical system and $j = 2$ represents the garnet/pyroxene system. The index i counts the phase changes in both mineralogical systems. v_j stands for the fraction of composition j in each affected grid.

2.3.2. Heat producing elements in the crust

Incompatible elements like the radiogenic isotopes tend to partition into melt phases. Thus, they are enriched in the resulting crustal material. This partitioning can have implications on the thermochemical evolution and should be taken into account (Hauck and Phillips, 2002). In the current model an enrichment of radiogenic elements in the crust of $\Lambda = 10$ is assumed (Taylor et al., 2006). It is described by the following linear relationship (Keller and Tackley, 2009):

$$H_r(c) = H_{mean}\frac{1 + c(\Lambda - 1)}{1 + c_{mean}(\Lambda - 1)} \tag{16}$$

where c is the composition varying from 0 (harzburgite) to 1 (basaltic crust). c_{mean} is the undepleted peridotite mantle, whereas H_{mean} is the mean radiogenic heating at the time of crust formation derived from the contributions of the lithophile elements.

2.3.3. Solidus temperature

The solidus temperature of the model reacts to mantle melting by linearly rising with the degree of depletion. Resulting, harzburgitic mantle material has a higher solidus temperature by 200 K than peridotitic mantle material at the same pressure conditions (McKenzie and Bickle, 1988).

Table 2
Phase transition properties as used in STAGYY.

i	Mineral	d (km)	T (K)	$\Delta\rho$ (kg m^{-3})	γ (MPa K^{-1})	$\Delta\eta$	w (km)
j = 1: Ol system							
1	ol → β-spinel	1007	1600	252	+2.5	20	51
2	β-spinel → γ-spinel	1173	1600	150	+5.0	1	85
3	γ-spinel → pv	1869	2260	400	−2.5	30	34
j = 2: Gt/Px system							
1	bas → ecl	158	0	350	0	1	34
2	gt/px → mj	1055	1600	150	+1.0	20	170
3	mj → pv	1869	2260	400	−2.5	30	170

3. Model setup

To test the hypothesis, we perform self-consistent two-dimensional numerical simulations of core formation and subsequent mantle convection. As an initial condition for the differentiation model, the planet is assumed to be fully accreted, yet not differentiated (see Golabek et al., 2009). This approach, where the extended accretion history is compressed into an initial condition, has the advantage of conserving the potential energy released by core formation. The resulting mantle temperature profile has the benefit of being spatially variable, yielding an early onset of mantle convection. The model box for the I2ELVIS simulation has a dimension of 8000×8000 km. The Mars-sized planetary body ($R_P = 3.4 \times 10^6$ m) is surrounded by a sticky air layer of zero density, constant temperature ($T_{SA} = 220$ K, corresponding to the martian mean surface temperature (Lodders and Fegley, 1998)) and constant viscosity ($\eta_{SA} = 10^{17}$ Pa s). This allows to simulate both a free surface, which can be of importance during core formation (Lin et al., 2009), and an infinite reservoir to absorb heat released from the planetary body. The employed grid resolution ranges from 401×401 to 801×801 nodal points. A resolution test shows no discernible influence on the model result.

For simplicity, isothermal initial temperature profiles close to the surface solidus temperature of peridotite ($T = 1100$–1500 K) are used (Reese and Solomatov, 2010). A dry olivine rheology (Ranalli, 1995) is applied as suggested by the analysis of SNC meteorites (e.g., Carr and Wänke, 1992) for Mars. This is reasonable as olivine represents the majority of the martian mantle composition and is weaker relative to pyroxenes, thus controlling mantle deformation (Mackwell, 1991).

As suggested for a Mars-like mantle composition, we apply a density cross-over between solid and molten silicates at 600 km depth ($P_{NB} \sim 6.5$ GPa) (Suzuki et al., 1998). For all models, we consider time-dependent radioactive heating by both short- and long-lived radiogenic isotopes. We assume that ^{40}K and ^{60}Fe partition into the iron core, whereas ^{26}Al, ^{235}U, ^{238}U, ^{232}Th remain in the martian mantle. Both codes take into account consumption, respectively release of latent heat due to melting and freezing of silicates and due to phase transitions.

Several hundred iron diapirs, each with 75 km radius, are initially randomly distributed throughout the planetary body (see Golabek et al., 2009). Additionally we assume that a giant impactor's iron core is large enough to penetrate into the martian mantle without being disrupted (Rubie et al., 2007; Dahl and Stevenson, 2010). The additional iron core of a giant impactor has a radius of 200–500 km. Assuming a H-chondrite composition, as proposed for Mars (Lodders and Fegley, 1997), this yields an original impactor body radius of ~430–1080 km (Ghosh and McSween, 1998; Scott, 2007). This is within the proposed size limits (Reese and Solomatov, 2006, 2010; Reese et al., 2010) for martian accretion. The total amount of iron added to the model setup will result in a core radius of ~1700 km. This lies within the range derived by inversion models based on the martian moment of inertia (Yoder et al., 2003; Khan and Connolly, 2008). The impact-induced temperature rise is constant in the isobaric core and decays exponentially at larger distances. All models of core formation are started at 5 Ma after CAI formation, which is within the time constraints for the formation of Mars (Raymond et al., 2006; Nimmo and Kleine, 2007).

We test the following setups (see Table 3):

The validity of the compressed initial condition has been tested in cases *0A* to *0E*. In these models the giant impact occurs after bulk core formation is finished. In these cases the giant impactor radius is kept constant at 500 km and its impact location is varied. No significant effect of the initial location of the giant impact or the temporal separation of events on the thermal structure can be identified (for more details see Supplemental material 1–5). Thus, the compressed initial condition seems to be a robust assumption to be used for the remainder of the study.

For case *1A* to *1T*, we include the giant impactor core already as an initial condition. In these models we vary systematically both the impactor core size r and the initial silicate temperature T. A reference Model 1 without a giant impact is computed as well (see Table 3).

From the melting history during core formation we derive in a postprocessing step a primordial crustal thickness distribution resulting from the final stages of magma ocean freezing. After core formation is complete, the silicate mantle temperature and the calculated primordial crust distribution resulting from the differentiation model are reinterpolated onto the spherical annulus grid used by STAGYY (Tackley, 2008; Hernlund and Tackley, 2008). There they serve as initial condition for the thermochemical mantle convection simulation. The mean temperature of the core is introduced as the lower thermal boundary condition into the flow calculation of STAGYY. The core temperature in the STAGYY simulation changes with time due to core cooling and time-dependent radiogenic heating by ^{60}Fe and ^{40}K. As standard resolution we use 1024×256 grid cells. Both, the bottom and the top boundary conditions are isothermal and free slip. Additionally, we include a slight viscosity stratification coupled to the phase changes in the martian mantle (Keller and Tackley, 2009) (see Table 2). Crust in the mantle convection simulation is self-consistently formed by melting of the garnet-pyroxene fraction in a pyrolitic mantle. The entire melt will be instantly erupted as basaltic crust to the surface. As an initial basalt fraction f_{bas} in the mantle we choose a value of 0.15 (Reese et al., 2010), which takes mantle depletion due to primordial crust formation during core formation into account. For all other physical parameters employed see Table 1.

4. Results

4.1. Best-fit model

In our best-fit Model *1L* (silicate temperature $T = 1300$ K, impactor core radius $r = 500$ km), we observe a runaway planetary differentiation process (Tonks and Melosh, 1993; Ricard et al., 2009)

Table 3
List of models.

Model	r (km)	T (K)	Comments
0A	0	1300	Separated core formation and giant impact, impact location 1
0B	0	1300	Separated core formation and giant impact, isothermal core, impact location 1
0C	0	1300	Separated core formation and giant impact, isothermal core, impact location 2
0D	0	1300	Separated core formation and giant impact, isothermal core, impact location 3
0E	0	1300	Separated core formation and giant impact, isothermal core, impact location 4
1	0	1300	Compressed initial condition, reference case without giant impactor core
1A	200	1100	Compressed initial condition
1B	300	1100	Compressed initial condition
1C	400	1100	Compressed initial condition
1D	500	1100	Compressed initial condition
1E	200	1200	Compressed initial condition
1F	300	1200	Compressed initial condition
1G	400	1200	Compressed initial condition
1H	500	1200	Compressed initial condition
1I	200	1300	Compressed initial condition
1J	300	1300	Compressed initial condition
1K	400	1300	Compressed initial condition
1L	500	1300	Compressed initial condition
1M	200	1400	Compressed initial condition
1N	300	1400	Compressed initial condition
1O	400	1400	Compressed initial condition
1P	500	1400	Compressed initial condition
1Q	200	1500	Compressed initial condition
1R	300	1500	Compressed initial condition
1S	400	1500	Compressed initial condition
1T	500	1500	Compressed initial condition

dominated by the sinking of the giant impactor's iron core through the mantle, lasting for less than 10 ka (see Fig. 1a). The amplitude of the impact heat combined with the shear heating induced by the sinking of the giant impactor core through the silicate mantle may well exceed the solidus of peridotite (see Fig. 1b). This facilitates the formation of a hemispherical magma ocean of several hundred kilometres depth that, with time, spreads out horizontally over the surface of the planet due to isostatic relaxation (Supplemental material 6). It solidifies again on a timescale of around 10–100 ka and forms a hemispherically asymmetrical primordial crust. Additionally, a thermal anomaly caused by the sinking of the giant impactor core (Ke and Solomatov, 2009) is formed in the mantle of the impacted hemisphere. Some melting also occurs on the opposite hemisphere. It is, however, not sufficient to produce comparable amounts of primordial crust.

After core formation is complete, the mantle is left with a hemispherically heterogeneous distribution in temperature. The thermal end state of the core formation models is now used as initial condition for the second model simulating the onset of mantle convection and further crust formation. In Fig. 2a, we observe that the thermal anomaly located in the deep mantle has an initial excess temperature of several hundred Kelvin. As a consequence this anomaly triggers a transient superplume that, due to decompression melting, produces a significant amount of additional crustal material confined to the region above the upwelling (see Fig. 2b).

Within the first 100–200 Ma after planetary differentiation, this upwelling supports the build-up of a massive volcanic province. After more than 100 Ma, the impact-induced plume slowly diminishes and a number of new upwellings form throughout the mantle. As by now, the lithosphere of the planet has reached a

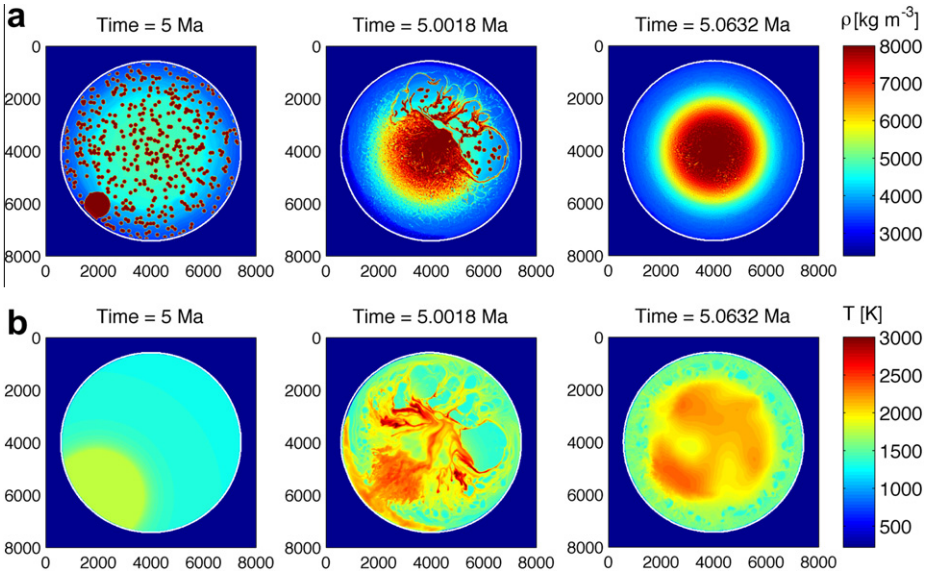

Fig. 1. Formation of a thermal anomaly due to the sinking of the giant impactor core during runaway differentiation. Evolution of (a) density and (b) temperature in a Mars-sized body at the time of core formation (Supplemental material 6).

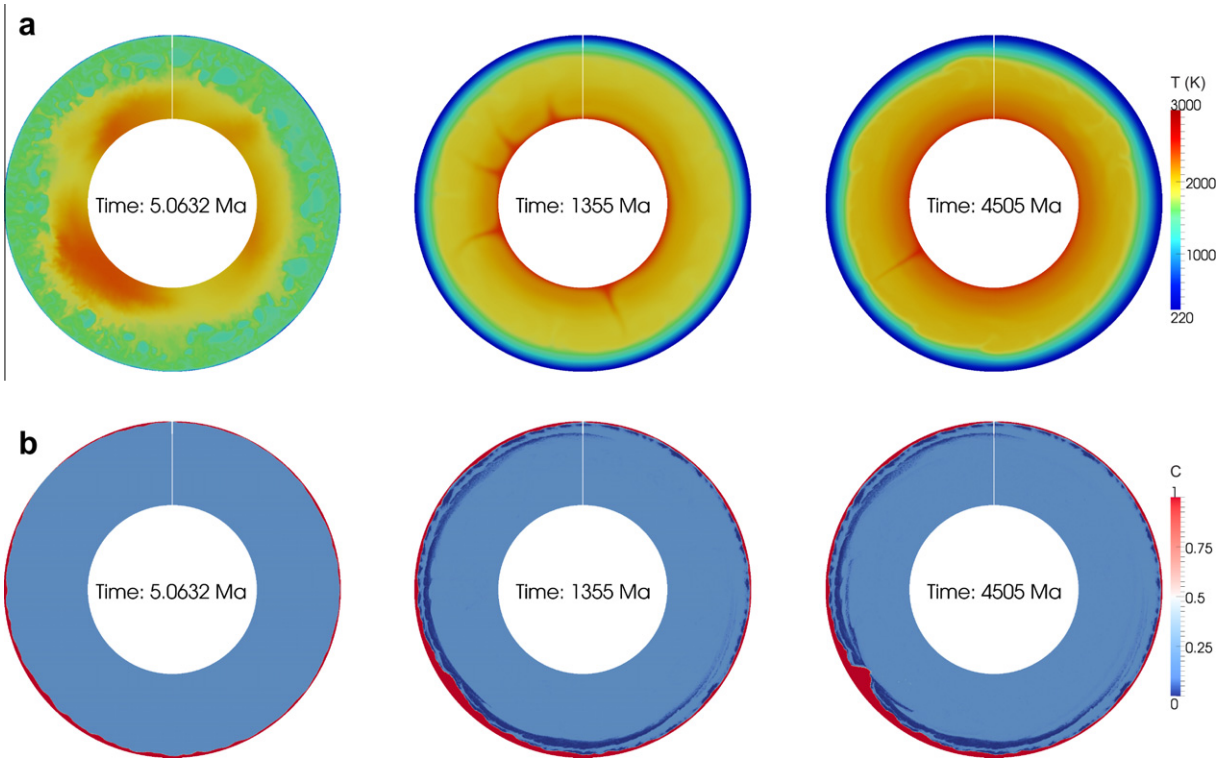

Fig. 2. Development of degree-1 convection during further planetary evolution. Time evolution of the (a) temperature and (b) composition field. In (b) blue color represents undepleted mantle material (peridotite), dark blue is depleted mantle (harzburgite), whereas crustal material (basalt) is given in red. The impact-induced thermal anomaly dominates the early mantle flow pattern in the first 100 Ma after core formation and produces significant amounts of new crust on the originally impacted hemisphere. Additional plumes exhibit insufficient excess temperatures to notably change the general crustal pattern during the later evolution. After 2.4 Ga one single plume is left beneath the early formed volcanic province, which supports limited volcanic activity. After 4.5 Ga evolution the compositional field still displays a crustal dichotomy between the hemispheres (Supplemental materials 7 and 8). (For interpretation of the references to color in this figure legend, the reader is referred to the web version of this article.)

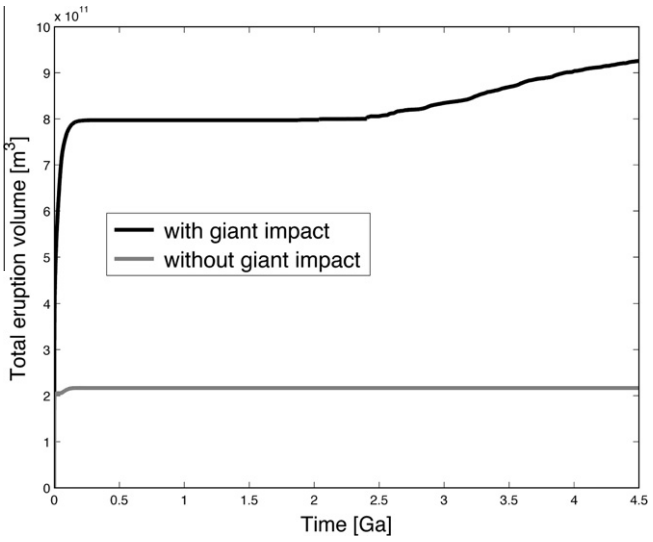

Fig. 3. Evolution of the total amount of erupted material over time. In the case including a giant impact (black line) we observe an early epoch of crust formation associated with magmatic activity during the first 100–200 Ma. Afterwards, the magmatic activity drops significantly, however it is sustained on a low level until present time. A model without a giant impact (grey line) produces only negligible amounts of crustal material as it remains magmatically inactive over the further planetary evolution.

considerable thickness, these new plumes are too weak to cause significant amounts of magmatism (see Figs. 2 and 3).

This long-term simulation encompassing the whole planetary evolution until the present time indicates that, as the lithospheric thickness increases with time, the dichotomous crustal distribution is preserved during the whole evolution of the planet. In general, the pattern of convection tends towards degree-1. However, due to the relatively low Rayleigh number of our model, it may take up to 2.4 Ga to collect all upwellings into only one.

The resulting crustal pattern after 4.5 Ga evolution shows a distribution with two peaks at around 40 and 55 km crustal thickness, respectively. It is in satisfactory agreement with the observed martian crustal distribution (Neumann et al., 2004) (see Fig. 4). For the present time, our models show a range of elastic lithospheric thicknesses comparable to observed values for both the martian poles and the Tharsis province (Grott and Breuer, 2010).

4.2. Influence of initial silicate temperature and the radius of the giant impactor core

As always when using simulations of this kind, the initial temperature of the planet's silicate mantle is the largest unknown. The size of the possible giant impactor is also uncertain (see above). A systematic study (see Table 3) is performed to study the influence of these two parameters.

Shear heating instabilities can form and can speed up the sinking of the giant impactor core (Golabek et al., 2009) as they reduce the silicate viscosity and increase sinking velocities (Weinberg and Podladchikov, 1994). This leads to runaway differentiation (see Fig. 1), which, however, is only possible when the giant impactor is large enough and/or the silicate temperature is sufficiently high (Ricard et al., 2009).

In the heated isobaric core the giant impactor iron core can in all cases easily induce shear heating instabilities. However, with further propagation towards the planetary centre, several factors

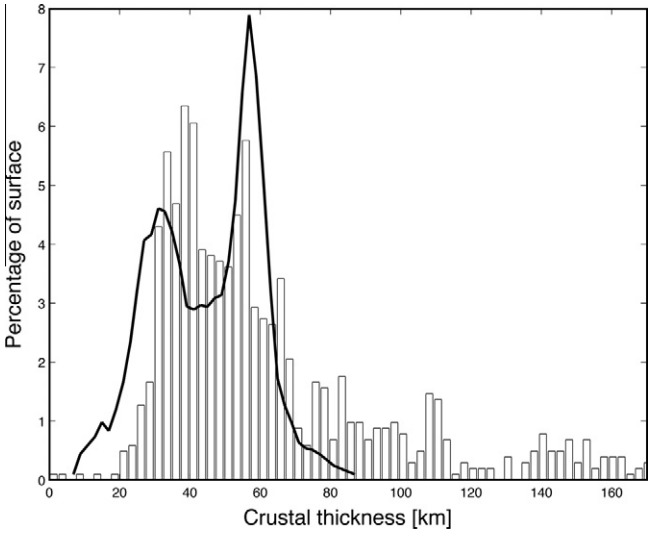

Fig. 4. Histogram of crustal distribution after 4.5 Ga model evolution. The model crust (bars) displays two peaks at around 40 and 55 km thickness comparable to the observed crustal thicknesses (Neumann et al., 2004) of the martian plains and southern highlands (black line).

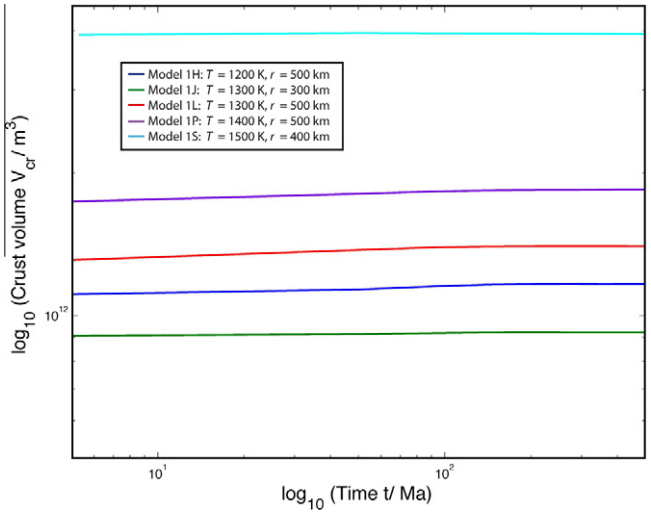

Fig. 5. Logarithmic plot of the influence of initial temperature profile and giant impactor core size on the final thickness of the primordial crust in the first 500 Ma after core formation. STAGYY measures crustal thickness at the depth where composition is $c = 0.5$. The high value chosen for potential crustal thickness may overestimate crustal thickness and thus also the crustal volume.

limit the ability to induce shear localization: The impact heating is reduced (see Eq. (3)), the viscosity increases due to its pressure dependency and finally, the gravitational acceleration is reduced. Thus, larger iron diapirs are needed to induce shear heating instabilities. Under these circumstances even large impactor cores cannot induce further shear heating instabilities in cold Models *1A–H* any more after sinking approximately to the bottom of the isobaric core.

Except for the smallest impactors, a hemispherical surface magma ocean can form due to the combined effect of impact heating and shear localization in the region of the isobaric core. In the deeper parts of cold planetary bodies, the sinking velocity of these cores is limited and no runaway differentiation can occur. Therefore, dissipated potential energy can be redistributed and no deep-seated thermal anomaly can develop in the mantle of the impacted hemisphere.

In contrast, in warm interiors the sufficiently large giant impactor cores can induce shear heating instabilities all the way to the planetary centre. This leads to the observed fast runaway differentiation and the formation of both a surface magma ocean and a hot wake in the mantle (Models *1K–1L*, *1O–P*, *1R–T*).

Fig. 5 shows that final crustal thickness increases with rising initial silicate temperature T (Hauck and Phillips, 2002; Breuer and Spohn, 2006). The crust can become thick enough as to reach the eclogite phase transition, leading to delamination of crust, thus limiting crustal thickness (see Fig. 5 Model (*1S*)). Nevertheless, the timescale of crust formation in models with equal-sized giant impactor cores is similar (see Fig. 5 Models *1H*, *1L* and *1P*). On the other hand, in Model *1J* crust formation ends earlier as less dissipated energy is available.

As shown by Fig. 6a and c the initial silicate temperature has a direct influence on the later mean CMB and mean silicate temperature. This is true not only just after core formation, but also during the further planetary evolution, thus controlling both the onset and the vigour of convection in the planetary body.

Fig. 6c shows that the radius of the giant impactor core can have an influence on the mean silicate temperature when the initial silicate temperature is the same (Models *1J* and *1L*). This can be explained by the larger area of the wake left behind by a larger iron core as the CMB temperatures of both models are nearly identical (see Fig. 6a), indicating similar excess temperatures due to the shear heating instabilities. Correspondingly, a larger impactor core in an initially colder mantle (Model *1L*) can lead to a similar mean temperature as obtained for a model with a smaller impactor core, but an initially warmer mantle (Model *1S*). The maximum temperatures at the CMB are, however, different with the initially warmer model having a higher CMB temperature.

Due to the inhomogeneity of the thermal field just after core formation and the rather low Rayleigh numbers of the models, a convergence in the mean temperature is not reached by 4.5 Ga (see Fig. 6c). Thus, the initial silicate temperature is the dominant factor controlling the planetary evolution until present time.

Fig. 6b and c shows that the timescale of rigid lid formation varies with the silicate temperature and thus depends on the Rayleigh number. This observation cannot be explained with the effect of crust formation only as the latter process happens on similar timescales for different models (see Fig. 5). Thus, a planet starting with a higher mantle temperature forms a thinner thermal boundary layer (Model *1S*) than a cooler planet (e.g., Model *1H*). After the rigid lid is established, the underlying planetary mantle will still be warm as only a relatively small fraction of the silicates cools down to form the lid. Due to the isolating effect of the rigid lid and core cooling, the planet will start to heat up. The importance of core cooling is confirmed by the change of slope of the temperature curves after roughly 1.5 Ga, corresponding to the half-life time of radiogenic potassium. This indicates that the ^{40}K heating conducted from the core is the most important contributor to mantle heating during the early evolution. Because of the high mantle temperature, the Rayleigh number increases and vigorous mantle convection establishes in Model *1S*. This leads, during the following evolution, to global secondary crust formation and magmatism not observed on real Mars.

On the other hand a planet starting at a cooler temperature (Model *1H*) will need longer to form its rigid lid as its thickness l is dependent on the Rayleigh number as $l \sim Ra^{-q}$ ($q \approx 1/3$) (Sotin and Labrosse, 1999; Deschamps et al., 2010) and the diffusion time approximating the lid formation time is $t_{diff} \sim l^2$. The large thickness of the rigid lid compared to the whole silicate area reduces the mean temperature of the silicates (see Fig. 6c). The drop of radiogenic heating in the core by the time the lid is established and the smaller thickness of the convecting layer compared to a warm case, lead to a reduction of the Rayleigh number. Thus, only

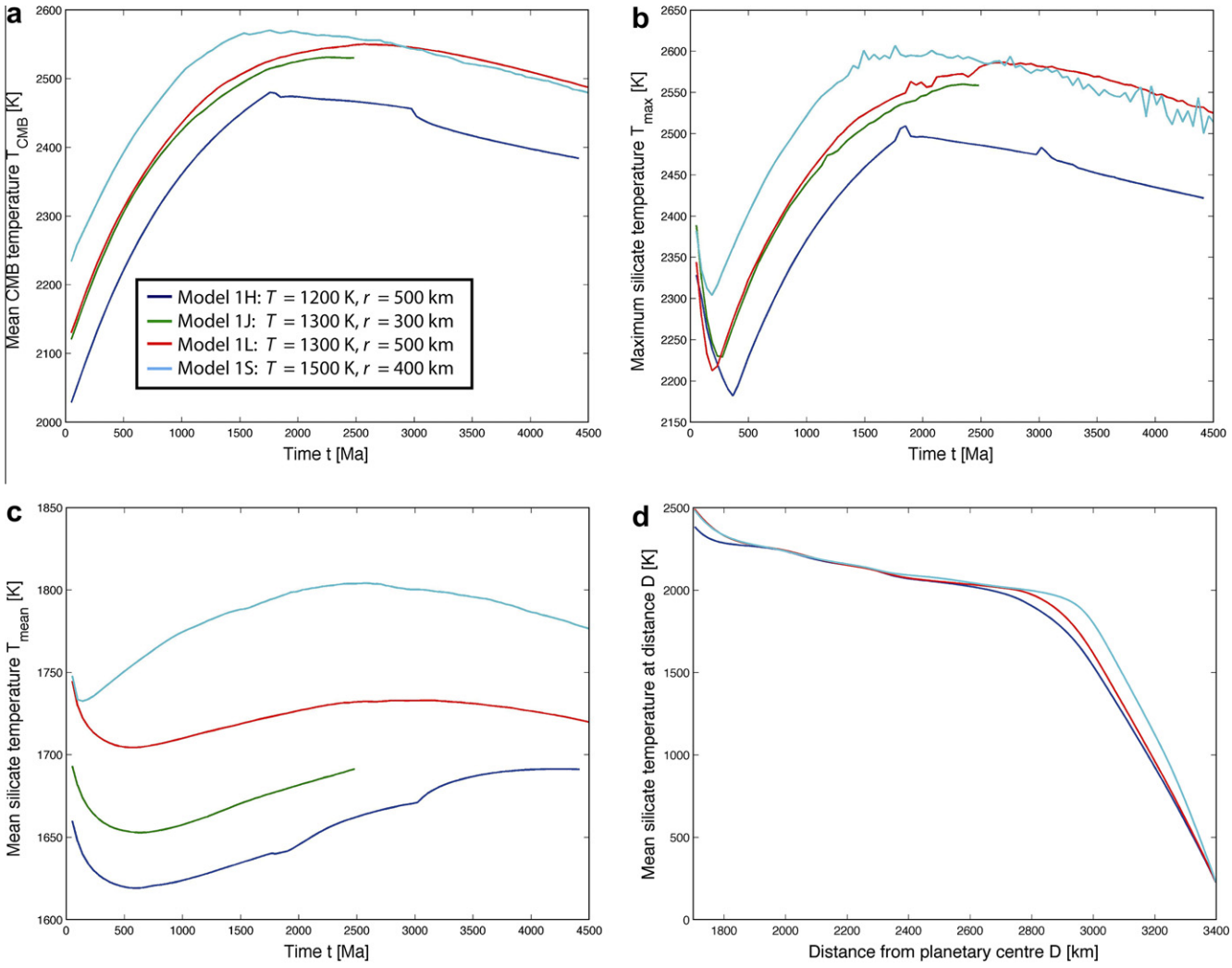

Fig. 6. Influence of initial temperature profile and giant impactor core size on the later thermochemical evolution. Development of (a) the CMB temperature, (b) the maximum and (c) the mean silicate temperature over time. (d) Comparison of thermal profiles after 4.415 Ga of evolution.

sluggish mantle convection is possible. This renders the planet unable to enter the stage of secondary crust formation (see Figs. 5 and 6d) and a surface composed of ancient basalts is preserved. Results indicate that only intermediate initial silicate temperatures (e.g. Model *1L*) can lead to a combination where the rigid lid is still thin enough that plumes with sufficient excess temperature can penetrate it. Only in this case the Rayleigh number reaches values supporting limited Mars-like magmatism leading to further volcanism (see Fig. 7).

5. Discussion

Core formation on Mars is expected to raise the mean temperature by 300 K (Solomon, 1979). Our models show that this temperature rise may be highly asymmetrical when the martian core formation involves a giant impact. This can lead to both an asymmetry in crustal thickness and thermal structure after core formation. Model results confirm that the initial silicate temperature is the dominant parameter, having effects on both the core formation and resulting mantle convection until recent times. Due to the low Rayleigh number of mantle convection in successful models, mean temperatures derived from different initial conditions temperatures do not converge even after 4.5 Ga of evolution. This indicates the possibility to use observations made for present-day Mars in order to obtain a better constraint on the initial temperature conditions.

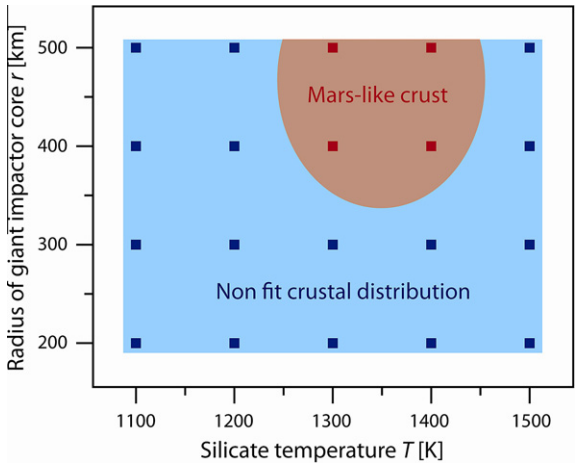

Fig. 7. A Mars-like dichotomous crustal distribution only forms for a certain range of initial silicate temperatures and impactor core radii. For low temperatures, insufficient amounts of crust are produced. Small impactor core radii do not induce a significant excess temperature anomaly on the impacted hemisphere. Hot planetary interiors, however, tend to produce a crustal thickness that is incompatible with geophysical measurements.

Our results agree with previous modelling efforts (Hauck and Phillips, 2002; Breuer and Spohn, 2006) and indicate that the bulk of the crustal structure exhibited on Mars today is ancient and dates to the earliest stages of planetary evolution. The proposal of the primordial crust derived from a magma ocean is consistent with the analysis of SNC meteorites from Mars (Norman, 1999). The timescale of bulk crust formation is 100–200 Ma, in agreement with the age of the crust on both hemispheres (Nimmo and Tanaka, 2005; Solomon et al., 2005; Frey, 2006).

The successful models demonstrate that, although the number and position of plumes is generally variable through time, one plume, into which eventually all other upwellings converge, usually stays stable underneath the thermally insulating crustal patch of the southern hemisphere and results in long-lived volcanism. This is consistent with arguments concerning the existence of a plume below Tharsis as presented by previous authors (Harder and Christensen, 1996; Zhong and Zuber, 2001; Wenzel et al., 2004; Roberts and Zhong, 2006; Li and Kiefer, 2007; Zhong, 2009; Keller and Tackley, 2009; Šrámek and Zhong, 2010). Moreover, the results suggest that, under favoured conditions, ongoing mantle convection and as observed, limited magmatism (Neukum et al., 2004; Werner, 2009; Carr and Head, 2010) are still viable on Mars today. Additionally, the amount of secondary crustal material generated by volcanism concentrated above the single upwelling in the successful models (see Fig. 3) is generally in agreement with estimations based on geochemical measurements indicating 20 ± 10% of secondary crust (Taylor and McLennan, 2009).

In conclusion, we find that the two-stage hypothesis for the origin of the crustal dichotomy and Tharsis has considerably more potential than the exogenic or endogenic hypotheses taken on their own. It operates not only within the geophysical and geochemical constraints for Mars, but also satisfies astrophysical limitations on martian accretion (Kokubo and Ida, 1996; Raymond et al., 2006). Thus, seen from the perspective of our models, the martian crust allows us to catch a uniquely direct glimpse of the very earliest stages of planetary evolution.

5.1. Model limitations

The current model has several limitations, which will be discussed here. The initial thermal condition for the presented calculations, the most important parameter controlling the further planetary evolution, remains uncertain. In reality, it results from the previous accretion and internal history of the protoplanet, which was not modelled here. The model setup is meant to conserve the energy as it compresses the whole accretion history into an initial condition. This model, however, overestimates the energy retention as it neglects the possibility of energy loss to space during earlier stages of planetary accretion.

Another limitation is that we do not know the silicate viscosity, because in diffusion creep viscosity depends on grain size, and this parameter is poorly known for Mars. Therefore, silicate viscosities are uncertain by at least a couple of orders of magnitude.

The basalt fraction f_{bas} is reduced at the beginning of the STAGYY simulation in the whole mantle to take previous depletion due to primordial crust formation into account. In reality, the mantle of the impacted hemisphere would be less fertile than on the other hemisphere, limiting later magmatism in the model.

Additionally, eruption efficiencies during both the magma ocean stage and during mantle convection are highly uncertain. Only for the stage of secondary crust formation values ranging from 5% (Kiefer, 2003) up to 80% (O'Neill et al., 2007) were suggested. Similar uncertainties can be expected for the primordial crust formation.

Another disadvantage of the model is that the primordial crust formation resulting from the freezing of the magma ocean is not incorporated self-consistently into I2ELVIS. Thus, no feedback of crust formation on the cooling of the surface magma ocean and the onset of mantle convection can take place. Also, possible breakup and subduction of the initially chill crust cannot be treated by this model. Therefore the primordial crust calculated in postprocessing can only be treated as an estimation of the upper limit of primordial crustal production.

Furthermore, the successful models form an ancient, Tharsis-like volcanic province located in the southern highlands. This location is inconsistent with the observed position of Tharsis at the dichotomy boundary. Yet, geological data suggest that the Tharsis plume migrated from an original early location in the Thaumasia region in the southern highlands towards the dichotomy boundary (Frey, 1979). Observing this migration of Tharsis in our 2D models is virtually impossible due to the geometrical restrictions. For obvious reasons of geometry, it is energetically more favourable for a spherical plume to adjust its position to the edge of the crustal dichotomy in 3D spherical geometry than in the 2D spherical annulus (Zhong, 2009; Šrámek and Zhong, 2010). Therefore, the prediction of our model that the upwelling responsible for the formation of Tharsis originates underneath the southern highlands and would afterwards migrate outwards is in good agreement with geological observations.

6. Conclusion

The two-stage hypothesis for the origin of the crustal dichotomy and Tharsis suggests that the martian crust would allow us to catch a uniquely direct glimpse at the very earliest stages of planetary evolution as the majority of the crustal structure we observe on Mars today requires its origin to be found in early transient processes. We infer that, imprinted in the martian crust, we witness the interplay of three of the most important processes shaping a young terrestrial planets' history: late giant impacts, planetary differentiation and the onset of mantle convection.

Acknowledgments

We thank the two reviewers, J. Hernlund, S. Labrosse and F. Deschamps for thoughtful comments, which helped to improve the manuscript. This work was financially supported by ETH Zürich, the Swiss National Science Foundation and the RF President Program Leading Scientific School of Russia.

Appendix A. Supplementary data

Supplementary data associated with this article can be found, in the online version, at doi:10.1016/j.icarus.2011.06.012.

References

Andrews-Hanna, J.C., Zuber, M.T., Banerdt, W.B., 2008. The Borealis basin and the origin of the martian crustal dichotomy. Nature 453, 1212–1215.
Bertka, C.M., Fei, Y., 1997. Mineralogy of the martian interior up to core–mantle boundary pressures. J. Geophys. Res. 102, 5251–5264.
Bottinga, Y., Weill, D.F., 1972. The viscosity of magmatic silicate liquids: A model for calculation. Am. J. Sci. 272, 438–475.
Breuer, D., Spohn, T., 2006. Viscosity of the martian mantle and its initial temperature: Constraints from crust formation history and the evolution of the magnetic field. Planet. Space Sci. 54, 153–169.
Bronstein, I.N., Semendjajew, K.A., Musiol, G., Mühlig, H. 2001. Taschenbuch der Mathematik, fifth ed., Harri Deutsch, Frankfurt am Main, 1191pp.
Burg, J.-P., Gerya, T.V., 2005. The role of viscous heating in Barrovian metamorphism of collisional orogens: Thermomechanical models and application to the Lepontine Dome in the Central Alps. J. Metamorp. Geol. 23, 75–95.
Carr, M.H., Head III, J.W., 2010. Geologic history of Mars. Earth Planet. Sci. Lett. 294, 185–203.
Carr, M.H., Wänke, H., 1992. Earth and Mars: Water inventories as clues to accretional histories. Icarus 98, 61–71.

Chambers, J.E., Wetherill, G.W., 1998. Making the terrestrial planets: N-body integrations of planetary embryos in three dimensions. Icarus 136, 304–327.
Connolly, J.A.D., 2005. Computation of phase equilibria by linear programming: A tool for geodynamic modeling and its application to subduction zone decarbonation. Earth Planet. Sci. Lett. 236, 524–541.
Croft, S.K., 1982. A first-order estimate of shock heating and vaporization in oceanic impacts. In: Silver, T.L., Schultz, P.H. (Eds.), Geological implications of impacts of large asteroids and comets on Earth. Spec. Pap. Geol. Soc. Am. 190, 143–152.
Dahl, T.W., Stevenson, D.J., 2010. Turbulent mixing of metal and silicate during planet accretion – And interpretation of the Hf-W chronometer. Earth Planet. Sci. Lett. 295, 177–186.
Deschamps, F., Tackley, P.J., Nakagawa, T., 2010. Temperature and heat flux scalings for isoviscous thermal convection in spherical geometry. Geophys. J. Int. 182, 137–154.
Frey, H.V., 1979. Thaumasia: A fossilized early forming Tharsis uplift. J. Geophys. Res. 84, 1009–1023.
Frey, H.V., 2006. Impact constraints on the age and origin of the lowlands of Mars. Geophys. Res. Lett. 33, L08S02.
Frey, H., Schultz, R.A., 1988. Large impact basins and the mega-impact origin for the crustal dichotomy on Mars. Geophys. Res. Lett. 15, 229–232.
Gerya, T.V., Yuen, D.A., 2007. Robust characteristics method for modelling multiphase visco–elasto-plastic thermo-mechanical problems. Phys. Earth Planet. Int. 163, 83–105.
Ghosh, A., McSween Jr., H.Y., 1998. A thermal model for the differentiation of asteroid 4 vesta, based on radiogenic heating. Icarus 134, 187–206.
Golabek, G.J., Gerya, T.V., Kaus, B.J.P., Ziethe, R., Tackley, P.J., 2009. Rheological controls on the terrestrial core formation mechanism. Geochem. Geophys. Geosyst. 10, Q11007.
Griffiths, R.W., Fink, J.H., 1993. Effects of surface cooling on the spreading of lava flows and domes. J. Fluid Mech. 252, 667–702.
Grott, M., Breuer, D., 2010. On the spatial variability of the martian elastic lithosphere thickness: Evidence for mantle plumes? J. Geophys. Res. 115, E03005.
Harder, H., Christensen, U.R., 1996. A one-plume model of martian mantle convection. Nature 380, 507–509.
Hauber, E., Grott, M., Kronberg, P., 2010. Martian rifts: Structural geology and geophysics. Earth Planet. Sci. Lett. 294, 393–410.
Hauck, S.A., Phillips, R.J., 2002. Thermal and crustal evolution of Mars. J. Geophys. Res. 107, 5052.
Hernlund, J.W., Tackley, P.J., 2008. Modeling mantle convection in the spherical annulus. Phys. Earth Planet. Int. 171, 48–54.
Hirschmann, M.M., 2000. Mantle solidus: Experimental constraints and the effects of peridotite composition. Geochem. Geophys. Geosyst. 1, 2000GC000070.
Ke, Y., Solomatov, V.S., 2009. Coupled core–mantle thermal evolution of early Mars. J. Geophys. Res. 114, E07004.
Keller, T., Tackley, P.J., 2009. Towards self-consistent modelling of the martian dichotomy: The influence of one-ridge convection on crustal thickness distribution. Icarus 202, 429–443.
Khan, A., Connolly, J.A.D., 2008. Constraining the composition and thermal state of Mars from inversion of geophysical data. J. Geophys. Res. 113, E07003.
Kiefer, W.S., 2003. Melting in the martian mantle: Shergottite formation and implications for present-day mantle convection on Mars. Meteorit. Planet. Sci. 39, 1815–1832.
Kokubo, E., Ida, S., 1996. On runaway growth of planetesimals. Icarus 123, 180–191.
Kraichnan, R.H., 1962. Turbulent thermal convection at arbitrary Prandtl number. Phys. Fluids 5, 1374–1389.
Li, Q., Kiefer, W.S., 2007. Mantle convection and magma production on present-day Mars: Effects of temperature-dependent rheology. Geophys. Res. Lett. 34, L16203.
Liebske, C., Schmickler, B., Terasaki, H., Poe, B.T., Suzuki, A., Funakoshi, K.-i., Ando, R., Rubie, D.C., 2005. Viscosity of peridotite liquid up to 13 GPa: Implications for magma ocean viscosities. Earth Planet. Sci. Lett. 240, 589–604.
Lin, J.-R., Gerya, T.V., Tackley, P.J., Yuen, D.A., Golabek, G.J., 2009. Numerical modeling of protocore destabilization during planetary accretion: Methodology and results. Icarus 204, 732–748.
Lodders, K., Fegley, B., 1997. An oxygen isotope model for the composition of Mars. Icarus 126, 373–394.
Lodders, K., Fegley, B., 1998. The Planetary Scientist's Companion. Oxford Univ. Press, New York, 371pp.
Mackwell, S.J., 1991. High-temperature rheology of enstatite: Implications for creep in the mantle. Geophys. Res. Lett. 18, 2027–2030.
Marinova, M.M., Aharonson, O., Asphaug, E., 2008. Mega-impact formation of the Mars hemispheric dichotomy. Nature 453, 1216–1219.
McCauley, J.F., Carr, M.H., Cutts, J.A., Hartmann, W.K., Masursky, H., Milton, D.J., Sharp, R.P., Wilhelms, D.E., 1972. Preliminary Mariner 9 report on the geology of Mars. Icarus 17, 289–327.
McKenzie, D., Bickle, M.J., 1988. The volume and composition of melt generated by extension of the lithosphere. J. Petrol. 29, 625–679.
Meade, C., Jeanloz, R., 1990. The strength of mantle silicates at high pressures and room temperature: Implications for the viscosity of the mantle. Nature 348, 533–535.
Monteux, J., Coltice, N., Dubuffet, F., Ricard, Y., 2007. Thermo-mechanical adjustment after impacts during planetary growth. Geophys. Res. Lett. 34, L24201.
Neukum, G. et al., 2004. Recent and episodic volcanic and glacial activity on Mars revealed by the High Resolution Stereo Camera. Nature 432, 971–979.
Neumann, G.A., Zuber, M.T., Wieczorek, M.A., McGovern, P.J., Lemoine, F.G., Smith, D.E., 2004. Crustal structure of Mars from gravity and topography. J. Geophys. Res. 109, E08002.
Niles, P.B., Boynton, W.V., Hoffman, J.H., Ming, D.W., Hamara, D., 2010. Stable isotope measurements of martian atmospheric CO_2 at the phoenix landing site. Science 329, 1334–1337.
Nimmo, F., Kleine, T., 2007. How rapidly did Mars accrete? Uncertainties in the Hf-W timing of core formation. Icarus 191, 497–504.
Nimmo, F., Tanaka, K., 2005. Early crustal evolution of Mars. Annu. Rev. Earth Planet. Sci. 33, 133–161.
Nimmo, F., Hart, S.D., Korycansky, D.G., Agnor, C.B., 2008. Implications of an impact origin for the martian hemispheric dichotomy. Nature 453, 1220–1223.
Norman, M.D., 1999. The composition and thickness of the crust of Mars estimated from rare Earth elements and neodymium-isotopic compositions of martian meteorites. Meteorit. Planet. Sci. 34, 439–449.
O'Keefe, J.D., Ahrens, T.J., 1977. Impact-induced energy partitioning, melting, and vaporization on terrestrial planets. Proc. Lunar Sci. Conf. 8, 3357–3374.
O'Neill, C., Lenardic, A., Jellinek, A.M., Kiefer, W.S., 2007. Melt propagation and volcanism in mantle convection simulations, with application for martian volcanic and atmospheric evolution. J. Geophys. Res. 112, E07003.
Phillips, R.J. et al., 2001. Ancient geodynamics and global-scale hydrology on Mars. Science 291, 2587–2591.
Pinkerton, H., Stevenson, R.J., 1992. Methods of determining the rheological properties of magmas at subliquidus temperatures, J. Volcanol. Geotherm. Res. 53, 47–66.
Ranalli, G., 1995. Rheology of the Earth, second ed., Chapman & Hall, London, UK, 436pp.
Raymond, S.N., Quinn, T., Lunine, J.I., 2006. High resolution simulations of the final assembly of Earth-like planets I. Terrestrial accretion and dynamics. Icarus 183, 265–282.
Reese, C.C., Solomatov, V.S., 2006. Fluid dynamics of local martian magma oceans. Icarus 184, 102–120.
Reese, C.C., Solomatov, V.S., 2010. Early martian dynamo generation due to giant impacts. Icarus 207, 82–97.
Reese, C.C., Solomatov, V.S., Baumgardner, J.R., 2002. Survival of impact-induced thermal anomalies in the martian mantle. J. Geophys. Res. 107, 5082.
Reese, C.C., Orth, C.P., Solomatov, V.S., 2010. Impact origin for the martian crustal dichotomy: Half-emptied or half-filled? J. Geophys. Res. 115, E05004.
Ricard, Y., Šrámek, O., Dubuffet, F., 2009. A multiphase model of runaway core–mantle segregation in planetary embryos. Earth Planet. Sci. Lett. 284, 144–150.
Roberts, J.H., Zhong, S., 2006. Degree-1 convection in the martian mantle and the origin of the hemispheric dichotomy. J. Geophys. Res. 111, E06013.
Rubie, D.C., Nimmo, F., Melosh, H.J., 2007. Formation of the Earth's core. In: Stevenson, D.J. (Ed.), Treatise on Geophysics, Evolution of the Earth, vol. 9. Elsevier B.V., Amsterdam, Netherlands, pp. 51–90.
Scott, E.R.D., 2007. Chondrites and the protoplanetary disk. Annu. Rev. Earth Planet. Sci. 35, 577–620.
Senshu, H., Kuramoto, K., Matsui, T., 2002. Thermal evolution of Mars. J. Geophys. Res. 107, 5118.
Siggia, E.D., 1994. High Rayleigh number convection. Annu. Rev Fluid Mech. 26, 137–168.
Solomatov, V.S., 2007. Magma oceans and primordial mantle differentiation. In: Stevenson, D.J. (Ed.), Treatise on Geophysics, Evolution of the Earth, vol. 9. Elsevier B.V., Amsterdam, Netherlands, pp. 91–119.
Solomon, S.C., 1979. Formation, history and energetics of cores in the terrestrial planets. Phys. Earth Planet. Int. 19, 168–192.
Solomon, S.C. et al., 2005. New perspectives on ancient Mars. Science 307, 1214–1220.
Sotin, C., Labrosse, S., 1999. Three-dimensional thermal convection in an isoviscous, infinite Prandtl number fluid heated from within and from below: Application to the transfer of heat through planetary mantles. Phys. Earth Planet. Int. 112, 171–190.
Šrámek, O., Zhong, S., 2010. Long-wavelength stagnant-lid convection with hemispheric variation in lithospheric thickness: Link between martian crustal dichotomy and Tharsis? J. Geophys. Res. 115, E09010.
Suzuki, A., Ohtani, E., Kato, T., 1998. Density and thermal expansion of a peridotite melt at high pressure. Phys. Earth Planet. Int. 107, 53–61.
Tackley, P.J., 2008. Modelling compressible mantle convection with large viscosity contrasts in a three-dimensional spherical shell using the yin-yang grid. Phys. Earth Planet. Int. 171, 7–18.
Tackley, P.J., Schubert, G., Glatzmaier, G.A., Schenk, P., Ratcliff, J.T., 2001. Three-dimensional simulations of mantle convection in Io. Icarus 149, 79–93.
Taylor, S.R., McLennan, S.M., 2009. Planetary Crusts: Their Composition, Origin and Evolution. Cambridge Univ. Press, Cambridge, UK, 404pp.
Taylor, G.J. et al., 2006. Bulk composition and early differentiation of Mars. J. Geophys. Res. 111, E03S10.
Tonks, W.B., Melosh, H.J., 1993. Magma ocean formation due to giant impacts. J. Geophys. Res. 98, 5319–5333.
Wade, J., Wood, B.J., 2005. Core formation and the oxidation state of the Earth. Earth Planet. Sci. Lett. 236, 78–95.
Weinberg, R.F., Podladchikov, Y., 1994. Diapiric ascent of magmas through power law crust and mantle. J. Geophys. Res. 99, 9543–9559.
Weinstein, S.A., 1995. The effects of a deep mantle endothermic phase change on the structure of thermal convection in silicate planets. J. Geophys. Res. 100, 11719–11728.

Wenzel, M.J., Manga, M., Jellinek, A.M., 2004. Tharsis as a consequence of Mars' dichotomy and layered mantle. Geophys. Res. Lett. 31, L04702.
Werner, S.C., 2009. The global martian volcanic evolutionary history. Icarus 201, 44–68.
Wetherill, G.W., 1992. An alternative model for the formation of the asteroids. Icarus 100, 307–325.
Wilhelms, D.E., Squyres, S.W., 1984. The martian dichotomy may be due to a giant impact. Nature 309, 138–140.
Yoder, C.F., Konopliv, A.S., Yuan, D.N., Standish, E.M., Folkner, W.M., 2003. Fluid core size of Mars from detection of the solar tide. Science 300, 299–303.
Zhong, S., 2009. Migration of Tharsis volcanism on Mars caused by differential rotation of the lithosphere. Nat. Geosci. 2, 19–23.
Zhong, S., Zuber, M.T., 2001. Degree-1 mantle convection and the crustal dichotomy on Mars. Earth Planet. Sci. Lett. 189, 75–84.